Contribution from the Institute for Molecular Science,
Myodaiji, Okazaki 444, Japan

Site-Selective Oxygen Exchange and Substitution of Organometallic Groups in an Amphiphilic Quadruple-Cubane-Type Cluster. Synthesis and Molecular Structure of $[(MCp^*)_4V_6O_{19}]$ (M = Rh, Ir)

Yoshihito Hayashi, Yoshiki Ozawa, and Kiyoshi Isobe*

Received July 12, 1990

Neutral organometallic oxide clusters $[(MCp^*)_4V_6O_{19}]$ (M = Rh (**1**), Ir (**2**); $Cp^* = \eta^5$-C_5Me_5) were synthesized by the reaction of $[MCp^*Cl_2]_2$ with sodium metavanadate in high yield (**1**, 90%; **2**, 96%). The structure has a quadruple-cubane-type framework, including the first vanadate hexamer with a V_6O_{19} core [Hayashi, Y.; Ozawa, Y.; Isobe, K. *Chem. Lett.* **1989**, 425]. The water suppression ^{17}O NMR spectrum of $[(RhCp^*)_4V_6O_{19}]$ enriched with ^{17}O showed that a site-selective oxygen exchange with free water occurs at the bridging oxygen atoms in the cluster without any change in its skeleton in the range of pH 6-8. Cluster **1** liberates sequentially $[RhCp^*(H_2O)_3]^{2+}$ groups in acidic water of pH <4. Treatment of this acidic aqueous solution with $[IrCp^*(H_2O)_3]^{2+}$ gave a mixture of clusters, $[(RhCp^*)_{4-n}(IrCp^*)_nV_6O_{19}]$ ($0 \le n \le 4$) (n = 1 (**3**), n = 2 (**4**), n = 3 (**5**)). These clusters were separated with a silica gel column and characterized by elemental analysis and IR and ^1H, ^{13}C, and ^{51}V NMR spectroscopies. **3** crystallizes in the orthorhombic space group *Pmmn* with a = 15.169 (3) Å, b = 18.632 (4) Å, c = 11.681 (1) Å, Z = 2, R = 0.046, and R_w = 0.0637 for 3432 reflections, that is, isomorphous with **1**. Although the location of the RhCp* and IrCp* groups in **3** was not specified by X-ray analysis due to their disorder, the chemical shifts of ^{51}V NMR spectra of **3** and the other mixed organometallic clusters clearly indicated that there is a magnetic nonequivalence between the vanadium atoms adjacent to the RhCp* group and those adjacent to the IrCp* group.

Introduction

Organometallic chemistry has been extended to the surfaces of metal oxides to form oxide-bound organometallic species that constitute a new and important area of heterogeneous catalysis.[1] Although X-ray absorption,[1c,2] photoelectron spectroscopy,[3] and other physical methods[4] gave many pieces of evidence that these species may have close analogues within coordination chemistry, the nature of the M-O bond and the influence of the metal oxide on the active site are really not understood.[5]

Recently, elucidation of the interaction of organometallic fragments with metal oxide surfaces has been carried out by theoretical studies employing tight-binding calculations of the extended Hückel type.[5] On the other hand, since the first polyanion bound covalently to an organometallic group, $[(Cp)Ti(PW_{11}O_{39})]^{4-}$ ($Cp = \eta^5$-C_5H_5) was reported by Klemperer in 1978,[6] experiments using heteropoly and isopoly oxometalate derivatives as model cluster compounds have been in progress. Thus a fairly large number of organometallic oxide clusters have been prepared and characterized. They are mainly classified into two groups:[7] the one group with organometallic attached to the κ^m-O (m = 1-3) site of polyoxoanions such as $W_{6-x}M_xO_{19}^{n-}$ (M = Nb, Ta, Ti),[8] $YW_{12-x}M_xO_{40}^{n-}$ (Y = Si; M = V, Nb),[7,9] and[10] $P_2W_{18-x}Nb_xO_{62}^{9-}$ and the other group with organometallics incorporated into the polyoxoanion framework of $M_5O_{18}^{6-}$ (M = Mo, W)[11] and $M_{11}YO_{39}^{n-}$ (M = Mo, W; Y = Si, P).[6,12] Various organometallic groups, for example, M'Cp, M'Cp*, M'(CO)$_3$, M'(C_6H_6), M'$(CO)_3$Sn, $[(PPh_3)_2M'H_2]_3$ (M' = Rh, Ti, Mn, Ru, Co, Ir), have been employed to assemble the oxide clusters that are anionic species soluble in polar solvents and solid materials insoluble in any solvent. The derivatives have metal oxide like structures and high molecular weights and interact with organometallic fragments to produce a surface mimicking those of heterogeneous metal oxides.[13] They have provided considerably useful structural data for understanding surfaces but limited data for the reactivities of M-O bonds[8a,14] and the active sites of organometallic fragments.[9b-e]

Recent in situ EXAFS[15] and FT-IR[16] studies show that RhCp* derivatives supported on inorganic oxide surface are more active and selective for hydroformylation than classical impregnation catalysts.

We have shown that some rational controls of charge, steric factors, and the number of the available coordination site on organometallic groups and oxometalates lead to formation of a novel neutral integrated cubane type of cluster, $[MCp^*M'O_4]_4$[17] and $[(MCp^*)_4V_6O_{19}]$[18] (M = Rh, Ir, M' = Mo, W), having three-dimensional frameworks of multimetal centers. These clusters catalyze the oxidation of cyclohexane with *t*-BuOOH in a unique fashion because of the mixed-metal center and prove to be good models for metal oxide surfaces.[19] We describe here the

(1) (a) Schwartz, J. *Acc. Chem. Res.* **1985**, *18*, 302. (b) Iwasawa, Y. In *Catalysis by Metal Complexes: Tailored Metal Catalyst*; Iwasawa, Y., Ed.; Reidel: Dordrecht, The Netherlands, 1986; p 1. (c) Lamb, H. H.; Gates, B. C.; Knözinger, H. *Angew. Chem., Int. Ed. Engl.* **1988**, *27*, 1127.
(2) Duivenvoorden, F. B. M.; Koningsberger, D. C.; Uh, Y. S.; Gates, B. C. *J. Am. Chem. Soc.* **1986**, *108*, 6254.
(3) Smith, P. B.; Bernasek, S. L.; Schwartz, J.; McNulty, G. S. *J. Am. Chem. Soc.* **1986**, *108*, 5654.
(4) Auger electron spectroscopy: see ref 3. IR spectroscopy: see ref 1c. Basu, P.; Panayotov, D.; Yates, J. T., Jr. *J. Am. Chem. Soc.* **1988**, *110*, 2074.
(5) Halet, J.-F.; Hoffmann, R. *J. Am. Chem. Soc.* **1989**, *111*, 3548.
(6) Ho, R. K. C.; Klemperer, W. G. *J. Am. Chem. Soc.* **1978**, *100*, 6772.
(7) Finke, R. G.; Rapko, B.; Domaille, P. J. *Organometallics* **1986**, *5*, 175.
(8) (a) Besecker, C. J.; Day, V. W.; Klemperer, W. G.; Thompson, M. R. *J. Am. Chem. Soc.* **1984**, *106*, 4125. (b) Day, V. W.; Klemperer, W. G.; Maltbie, D. J. *Organometallics* **1985**, *4*, 104. (c) Besecker, C. J.; Day, V. W.; Klemperer, W. G.; Thompson, M. R. *Inorg. Chem.* **1985**, *24*, 44. (d) Day, V. W.; Earley, C. W.; Klemperer, W. G.; Maltbie, D. J. *J. Am. Chem. Soc.* **1985**, *107*, 8261. (e) Besecker, C. J.; Klemperer, W. G.; Day, V. W. *J. Am. Chem. Soc.* **1982**, *104*, 6158.
(9) (a) Finke, R. G.; Droege, M. W. *J. Am. Chem. Soc.* **1984**, *106*, 7274. (b) Siedle, A. R.; Markell, C. G.; Lyon, P. A.; Hodgson, K. O.; Roe, A. L. *Inorg. Chem.* **1987**, *26*, 219. (c) Siedle, A. R.; Newmark, R. A. *J. Am. Chem. Soc.* **1989**, *111*, 2058. (d) Siedle, A. R.; Newmark, R. A.; Sahyun, M. R. V.; Lyon, P. A.; Hunt, S. L.; Skarjune, R. P. *J. Am. Chem. Soc.* **1989**, *111*, 8346. (e) Siedle, A. R.; Newmark, R. A. *Organometallics* **1989**, *8*, 1442.
(10) Edlund, D. J.; Saxton, R. J.; Lyon, D. K.; Finke, R. G. *Organometallics* **1988**, *7*, 1692.
(11) Che, T. M.; Day, V. W.; Francesconi, L. C.; Fredrich, M. F.; Klemperer, W. G.; Shum, W. *Inorg. Chem.* **1985**, *24*, 4055.
(12) Knoth, W. H.; *J. Am. Chem. Soc.* **1979**, *101*, 2211.
(13) Pope, M. T. *Heteropoly and Isopoly Oxometalates*; Inorganic Chemistry Concepts No. 8; Springer-Verlag: Berlin, Heidelberg, New York, Tokyo, 1983; pp 118-127.
(14) Day, V. W.; Fredrich, M. F.; Thompson, M. R.; Klemperer, W. G.; Liu, R.-S.; Shum, W. *J. Am. Chem. Soc.* **1981**, *103*, 3597.
(15) Asakura, K.; Kitamura-Bando, K.; Isobe, K.; Arakawa, H.; Iwasawa, Y. *J. Am. Chem. Soc.* **1990**, *112*, 3242.
(16) Kitamura-Bando, K.; Asakura, K.; Arakawa, H.; Sugi, Y.; Isobe, K.; Iwasawa, Y. *J. Chem. Soc., Chem. Commun.* **1990**, 253.
(17) Hayashi, Y.; Toriumu, K.; Isobe, K. *J. Am. Chem. Soc.* **1988**, *110*, 3666.
(18) Preliminary results for $[(RhCp^*)_4V_6O_{19}]$ were communicated previously by our group and Klemperer's group independently at the same time: (a) Hayashi, Y.; Ozawa, Y.; Isobe, K. *Chem. Lett.* **1989**, 425. (b) Chae, H. K.; Klemperer, W. G.; Day, V. W. *Inorg. Chem.* **1989**, *28*, 1423.
(19) Zhang, C.; Ozawa, Y.; Hayashi, Y.; Isobe, K. *J. Organomet. Chem.* **1989**, *373*, C21.

0020-1669/91/1330-1025$02.50/0

quadruple-cubane-type cluster $[(MCp^*)_4V_6O_{19}]$, with focus on the nature of the metal–oxygen bond influenced by the organometallic groups, and show some basic chemistries with respect to the oxide-bound organometallic species.

Experimental Section

Reagents, Solvents, and General Procedures. The following chemicals were purchased from commercial sources and used without further purification: $RhCl_3·3H_2O$ (Tanaka Kikinzoku); $IrCl_3·nH_2O$ (Mituwa Chemicals); pentamethylcyclopentadiene (Aldrich); $NaVO_3$ (Wako); $AgPF_6$ (Aldrich); 40% HBF_4 aqueous solution (Wako); 60% $HClO_4$ (Wako); 25–40 mesh LiChroprep (Merck); 10% ^{17}O-enriched water (CEA). Dichloromethane was distilled over CaH_2 (Wako) under Ar. Methanol was distilled under Ar. $[MCp^*Cl_2]_2$ (M = Rh, Ir) was synthesized according to a modified literature procedure[20] using pentamethylcyclopentadiene instead of Dewar benzene.

Analytical Procedures. Elemental analyses were performed by IMS Chemical Material Center. Infrared spectra were measured in mineral oil between KRS-5 plates on a Hitachi 270-30 infrared spectrometer. ^1H, ^{13}C, ^{17}O, and ^{51}V NMR spectra were recorded on a JEOL GX 400 spectrometer in $CDCl_3$, CD_2Cl_2, or D_2O. These chemical shifts were referenced to TMS (^1H and ^{13}C). Secondary ionization mass spectroscopy (SIMS) spectra were recorded on a HITAC M4000 high-resolution double-focusing mass spectrometer. Milligram samples were dissolved in 100 μL of CH_3OH, and 1–2 μL of this solution was then added to 10 μL of *m*-nitrobenzyl alcohol matrix placed on the target. An 8-kV Xe^+ ion beam was used to bombard the target matrix, and positive ions produced were detected.

Preparation of $[(RhCp^*)_4V_6O_{19}]$ (1). A suspension of $[RhCp^*Cl_2]_2$ (321 mg, 5.19×10^{-4} mol) in 10 cm^3 of water (pH 3.5) was added dropwise to an aqueous suspension (10 cm^3) of $NaVO_3$ (633 mg, 5.19×10^{-3} mol). After the mixture was stirred for 30 min, the pH of the solution rose to 6.8. The resulting deep red solution was extracted with 20 cm^3 of dichloromethane, the organic layer was collected and dried over Na_2SO_4, giving a red black powder on evaporation of the solvent (364 mg, 89.7% yield). The compound contains four water molecules of crystallization, which are removed under vacuum at room temperature. IR 1080, 1028, 936 [$\nu(V–O^T)$], 686, 562 [$\nu(V–O^B)$], 484 [$\nu(V–O^C)$] cm^{-1} (O^T = terminal oxygen, O^B = bridging oxygen, O^C = central oxygen). ^1H NMR ($CDCl_3$): δ 1.939 (s, $C_5(CH_3)_5$, (D_2O) δ 1.23 (s, $C_5(CH_3)_5$). $^{13}C\{^1H\}$ NMR ($CDCl_3$): δ 93.72 (d, $C_5(CH_3)_5$, J_{C-Rh} = 8.9 Hz), 9.44 (s, $C_5(CH_3)_5$), (D_2O) δ 96.22 (d, $C_5(CH_3)_5$, J_{C-Rh} = 9.1 Hz), 8.64 (s, $C_5(CH_3)_5$). ^{17}O NMR ($CDCl_3$): δ 1213 (O^T, 470-Hz half-width), 386 (O^B, 767-Hz half-width), 27 (O^C, 12-Hz half-width), (D_2O) δ 1176 (O^T, 525-Hz half-width), 404 (O^B, 1192-Hz half-width), 27 (O^C, 14-Hz half-width). ^{51}V NMR (CD_2Cl_2): δ −512[21] (305-Hz half-width), (D_2O) δ −511 (540-Hz half-width). Anal. Calcd for $C_{40}H_{60}O_{19}Rh_4V_6$: C, 30.75; H, 3.87. Found: C, 30.59; H, 4.28. MS (SIMS): calcd for $C_{40}H_{60}O_{19}Rh_4V_6$, 1562 (the most abundant mass ion); found, *m/z* 1563 (MH^+), 1546 ($M - O^+$), 1530 ($M - 2O^+$).

Preparation of $[(IrCp^*)_4V_6O_{19}]$ (2). The procedure was similar to that described for **1**. $[IrCp^*Cl_2]_2$ (210 mg, 2.63×10^{-4} mol) afforded 242 mg of $[(IrCp^*)_4V_6O_{19}]$ (95.7% yield). IR 1078, 1034, 940 [$\nu(V–O^T)$], 748, 672, 562 [$\nu(V–O^B)$], 500 [$\nu(V–O^C)$] cm^{-1}. ^1H NMR ($CDCl_3$): δ 1.897 (s, $C_5(CH_3)_5$): $^{13}C\{^1H\}$ NMR ($CDCl_3$): δ 87.06 (s, $C_5(CH_3)_5$), 9.78 (s, $C_5(CH_3)_5$). ^{17}O NMR ($CDCl_3$): δ 1236 (O^T, 388-Hz half-width), 360 (O^B, 883-Hz half-width), 37 (O^C, 16-Hz half-width); ^{51}V NMR (CD_2Cl_2) δ −529 (375-Hz half-width). Anal. Calcd for $C_{40}H_{60}Ir_4O_{19}V_6$: C, 25.03; H, 3.15. Found: C, 25.26; H, 3.45. MS (SIMS): calcd for $C_{40}H_{60}Ir_4O_{19}V_6$: 1920 (the most abundant mass ion); found, *m/z* 1921 (MH^+), 1904 ($M - O^+$), 1888 ($M - 2O^+$).

Preparation of $[(RhCp^*)_{4-n}(IrCp^*)_nV_6O_{19}]$ ($1 \le n \le 3$; n = 1 (3), n = 2 (4), n = 3 (5)). Method a. To a vigorously stirred acidic aqueous solution of $[IrCp^*Cl_2]_2$ (147 mg, 1.85×10^{-3} mol in 10 cm^3 of water), $AgPF_6$ (187 mg, 7.40×10^{-3} mol in 5 cm^3 of water) was added and AgCl was precipitated immediately. After the solution was stirred for ca. 30 min, AgCl was filtered off and the resulting acidic solution of[22] $[(IrCp^*)(H_2O)_3]^{2+}$ was dropped into an aqueous solution of cluster **1** (288 mg, 1.84×10^{-3} mol in 10 cm^3 of water). After the solution was stirred for 1 h, a deep red solution was extracted with 50 cm^3 of dichloromethane and the organic layer was concentrated to 10 cm^3 and dried over Na_2SO_4. The total yield of the crude material was 310 mg.

Method b. $[RhCp^*Cl_2]_2$ (210 mg, 3.40×10^{-4} mol) and $[IrCp^*Cl_2]_2$ (210 mg, 2.64×10^{-4} mol) were suspended in 10 cm^3 of water and treated with an aqueous solution of $NaVO_3$ (633 mg, 5.19×10^{-3} mol) in 10 cm^3 of water. The mixture was stirred for ca. 30 min until the pH of the solution increased to 6.7. The resulting deep red solution was extracted with 30 cm^3 of dichloromethane, and then the organic layer was collected and dried with Na_2SO_4, giving a crude red black powder product on evaporation of the solvent (364 mg).

Separation. The crude product comprised of the mixture of $[(RhCp^*)_{4-n}(IrCp^*)_nV_6O_{19}]$ ($0 \le n \le 4$) (50 mg) from method a was dissolved in a minimum of dichloromethane and chromatographed on a silica gel column (Merck, 25–40 mesh LiChroprep 60, o.d. = 5 cm, height = 30 cm) using medium pressure liquid chromatography (Yamazen). Elution with CH_2Cl_2/acetone/methanol (10:10:1 by volume) gave five purple fractions, which separately contained clusters **2**, **5**, **4**, **3**, and **1**, in that order. Each fraction was dried with Na_2SO_4 and evaporated to give 2–10 mg of the substituted clusters. Every reaction gave a mixture of all clusters of $[(RhCp^*)_{4-n}(IrCp^*)_nV_6O_{19}]$ ($0 \le n \le 4$). When the Rh/Ir gram equivalent ratio of the starting materials was varied to 3:1, 2:2, and 1:3, then each reaction afforded **3**, **4**, and **5** as a main product, respectively. The yields of the isolated clusters changed from 3 to 20% with the reaction and separation conditions (the yields are based on the V_6O_{19} fragment in **1**), and all clusters gave satisfactory elemental analysis (vide infra).

(a) $[(RhCp^*)_3(IrCp^*)V_6O_{19}]$ (3). IR 1078, 1030, 936 [$\nu(V–O^T)$], 678 [$\nu(V–O^B)$], 562 [$\nu(V–O^B)$], 492 [$\nu(V–O^C)$] cm^{-1}. ^1H NMR ($CDCl_3$): δ 1.944 (s, $RhC_5(CH_3)_5$), 1.880 (s, $IrC_5(CH_3)_5$). $^{13}C\{^1H\}$ NMR ($CDCl_3$): δ 94.44 (d, $RhC_5(CH_3)_5$, J_{C-Rh} = 11.1 Hz), 86.05 (s, $IrC_5(CH_3)_5$), 9.99 (s, $IrC_5(CH_3)_5$), 9.53 (s, $RhC_5(CH_3)_5$). ^{51}V NMR (CD_2Cl_2): δ −511 (340-Hz half-width), −517 (366-Hz half-width). Anal. Calcd for $C_{40}H_{60}IrO_{19}Rh_3V_6$: C, 29.09; H, 3.66. Found: C, 29.00; H, 4.28.

(b) $[(RhCp^*)_2(IrCp^*)_2V_6O_{19}]$ (4). IR 1076, 1031, 938 [$\nu(V–O^T)$], 676 [$\nu(V–O^B)$], 560 [$\nu(V–O^B)$], 494 [$\nu(V–O^C)$] cm^{-1}. ^1H NMR ($CDCl_3$): δ 1.949 (s, $RhC_5(CH_3)_5$), 1.885 (s, $IrC_5(CH_3)_5$). $^{13}C\{^1H\}$ NMR ($CDCl_3$): δ 94.83 (d, $RhC_5(CH_3)_5$, J_{C-Rh} = 9.2 Hz), 87.06 (s, $IrC_5(CH_3)_5$), 9.95 (s, $IrC_5(CH_3)_5$), 9.51 (s, $RhC_5(CH_3)_5$). ^{51}V NMR (CD_2Cl_2): δ −511 (419-Hz half-width), −518 (366-Hz half-width), −527 (419-Hz half-width). Anal. Calcd for $C_{43}H_{66}Ir_2O_{20}Rh_2V_6$ (**4**·$(CH_3)_2CO$): (**3**·$(CH_3)_2CO$): C, 28.71; H, 3.70. Found: C, 28.47; H, 3.80.

(c) $[(RhCp^*)(IrCp^*)_3V_6O_{19}]$ (5). IR 1078, 1033, 940 [$\nu(V–O^T)$], 672 [$\nu(V–O^B)$], 560 [$\nu(V–O^B)$], 495 [$\nu(V–O^C)$] cm^{-1}. ^1H NMR ($CDCl_3$): δ 1.953 (s, $RhC_5(CH_3)_5$), 1.891 (s, $IrC_5(CH_3)_5$). $^{13}C\{^1H\}$ NMR ($CDCl_3$): δ 94.83 (d, $RhC_5(CH_3)_5$, J_{C-Rh} = 9.2 Hz), 87.06 (s, $IrC_5(CH_3)_5$), 9.78 (s, $IrC_5(CH_3)_5$), 9.33 (s, $RhC_5(CH_3)_5$). ^{51}V NMR (CD_2Cl_2): δ −518 (366-Hz half-width), −527 (375-Hz half-width). Anal. Calcd for $C_{40}H_{60}Ir_3O_{19}RhV_6$: C, 26.25; H, 3.30. Found: C, 26.05; H, 3.71.

^{17}O and ^{51}V NMR Analyses. ^{17}O and ^{51}V NMR chemical shifts were referenced externally to D_2O (^{17}O) and neat $VOCl_3$ (^{51}V) (Wako) at 20 °C, respectively, by a sample replacement method. Chemical shifts for all nuclei are reported as positive numbers for resonances that are observed at higher frequency (lower field) than the references. Typical ^{17}O spectral parameters are as follows: spectrometer frequency = 54.2 MHz, sweep width = 150–190 kHz, pulse delay = 120 μs, predelay = 0.2 ms, and pulse width = 18.3 μs. ^{51}V spectral parameters are as follows: spectrometer frequency = 105.1 MHz, sweep width = 143 kHz, pulse delay = 0.16 s, predelay = 0.2 ms, and pulse width = 14.3 μs.

^{17}O-Enrichment Procedures. In order to enrich all oxygen sites in $[(RhCp^*)_4V_6O_{19}]$ with ^{17}O, the starting material, $NaVO_3$, was first treated with ^{17}O-enriched water. $NaVO_3$ (412 mg, 3.38×10^{-3} mol) suspended in 1 cm^3 of 10% enriched $H_2{}^{17}O$ in a 2-cm^3 vial was heated at 90 °C for 3 h with stirring and cooled to 25 °C. To the resulting solution $[RhCp^*Cl_2]_2$ (373 mg, 6.03×10^{-4} mol) and 0.5 cm^3 of 10% enriched water were added and then the mixture was heated to 95 °C with vigorous stirring. After the solution was heated for 3 h with stirring, the solvent was removed to dryness, and the enriched water was recovered. A residual black solid was extracted with dichloromethane (5 × 5 cm^3), and the collected solution was dried over Na_2SO_4. The solvent was evaporated under vacuum to yield ca. 10% ^{17}O-enriched $[(RhCp^*)_4V_6{}^{17}O_{19}]$(**1**–$^{17}O$) (463 mg, 98% yield). The ^{17}O-enriched $[(IrCp^*)_4V_6{}^{17}O_{19}]$(**2**–$^{17}O$) was prepared by a method similar to that for **1**–^{17}O.

(20) Kang, J. W.; Moseley, K.; Maitlis, P. M. *J. Am. Chem. Soc.* **1969**, *91*, 5970.

(21) We reported previously the value of the ^{51}V NMR chemical shift of **1** as δ 648 in ref 18a. This value is incorrect. The correct value is δ −512, as shown in the text. We thank Professor Klemperer for informing us of his correct result.

(22) We did not isolate this complex, but for preparation we used acidic conditions to avoid contamination of $[(IrCp^*)_2(OH)_3]^+$.[23] Treatment of the aqueous solution of $[(IrCp^*)(H_2O)_3]^{2+}$ with benzene afforded $[IrCp^*(\eta^6\text{-}C_6H_6)]^{2+}$.[24]

(23) Carmona, D.; Oro, L. A.; Lamata, M. P.; Puebla, M. P.; Ruiz, J.; Maitlis, P. M. *J. Chem. Soc., Dalton Trans.* **1987**, 639.

(24) Grundy, S. L.; Smith, A. J.; Adams, H.; Maitlis, P. M. *J. Chem. Soc., Dalton Trans.* **1984**, 1747.

Table I. Crystallographic Data for $1{\cdot}3CH_3CN{\cdot}H_2O$ and $3{\cdot}3CH_3CN{\cdot}H_2O$

	$1{\cdot}3CH_3CN{\cdot}H_2O$	$3{\cdot}3CH_3CN{\cdot}H_2O$
formula	$C_{46}H_{71}N_3O_{20}Rh_4V_6$	$C_{46}H_{71}IrN_3O_{20}Rh_3V_6$
mol wt	1703.3	1792.7
cryst syst	orthorhombic	orthorhombic
a, Å	15.151 (2)	15.169 (3)
b, Å	18.611 (2)	18.632 (4)
c, Å	11.682 (2)	11.681 (1)
V, Å^3	3294.2 (7)	3301.3 (9)
space group	*Pmmn* (No. 59)	*Pmmn* (No. 59)
Z	2	2
λ(Mo Kα), Å	0.71073, graphite monochromator	0.71073, graphite monochromator
D(calcd), g cm^{-3}	1.72	1.80
μ(Mo Kα), cm^{-1}	18.7	37.5
no. of obsd reflecns	1484 ($\|F_o\| > 3\sigma(F_o)$)	3432 ($\|F_o\| > 6\sigma(F_o)$)
R	0.0460	0.0482
R_w	0.0637	0.0656

Study of pH Dependence of Cluster 1 in D_2O. The pH dependence of the ^1H NMR spectra of cluster **1** was examined at 20 °C by using a 2-cm^3 solution of cluster **1** (31 mg) in D_2O and adjusting the pH with 1 M HBF_4. Six kinds of different pH samples were prepared at pH 7.1, 4.8, 3.8, 2.8, 1.6, and 1.0 and were subjected to ^1H NMR assay for observation of the dissociation reaction. The pH values of the solutions were determined after bubbling in Ar gas for several minutes. The chemical shifts of[25] $[(RhCp^*)(D_2O)_3]^{2+}$ and cluster **1** in D_2O were preconfirmed from the authentic samples.[26]

Study of ^{17}O-Exchange Reaction of Cluster 1–^{17}O in D_2O. The ^{17}O-enriched cluster **1** (**1**–^{17}O) (24 mg, 1.5×10^{-5} mol) was dissolved in D_2O (3 cm^3) at room temperature to make a nearly saturated solution, and the sample solution was warmed in a constant-temperature bath at 60, 70, and 90 °C. The **1**–^{17}O solution displayed a pH of 6.8 without the addition of a buffer and remained essentially constant for the oxygen exchange run (approximately 4 h). Therefore, to study the exchange at a constant pH of ca. 7, it was not necessary to have a buffer present. The oxygen-exchange reaction of cluster **1** did not proceed at room temperature during a few weeks. Therefore, the measurement of the NMR spectrum was carried out at 20 °C to quench the reaction. The water suppression spectra of ^{17}O were measured with a selective excitation method (one-to-one pulse sequences) using a 45° pulse at 89-ms-pulse intervals.[27] The signal-to-noise ratio was enhanced by a 15-Hz exponential line broadening function. All ^{17}O-exchange reactions were performed under the same conditions: the sweep width (185 185 Hz), the pulse width (18.3 μs), the acquisition time (0.022 s), and the FID were accumulated for 100 000 pulses. We should point out that the methods for observing the oxygen-exchange reaction of oxide clusters with bulk water by ^{17}O NMR spectroscopy are limited because of a large water peak. However, there are some examples in which the oxygen-exchange reaction is followed by ^{17}O NMR measurement using a relaxation agent to suppress the bulk water peak,[28] with a high concentration of the ^{17}O-enriched sample[29] and a small amount of water added to the organic solution.[30] Here we employed a direct method to observe the oxygen-exchange reaction in aqueous solution, using a selectively excited hard-pulse method for convenience and circumventing the addition of agents to the solution of the sample.

X-ray Structure Determination. $[(RhCp^*)_4V_6O_{19}]{\cdot}3CH_3CN{\cdot}H_2O$ ($1{\cdot}3CH_3CN{\cdot}H_2O$). A black cubic crystal of cluster $1{\cdot}3CH_3CN{\cdot}H_2O$ (0.12 × 0.18 × 0.11 mm) recrystallized from acetonitrile was sealed with mother liquor in a thin-walled glass capillary (0.5-mm diameter). Intensity data were collected on a RIGAKU AFC-5 four-circle diffractometer at 25 °C using the θ–2θ scan technique and graphite-monochromated Mo Kα radiation (λ = 0.71073 Å). The intensities for reflections were corrected for Lorentz–polarization factors and the absorption effect but not for extinction. The cell dimensions were determined by least-squares fitting of 25 centered reflections ($25° < 2\theta < 30°$). Crystallographic data are listed in Table I, and fractional coordinates are listed in Table II.

Table II. Fractional Coordinates (×10^5 for Metal Atoms, ×10^4 for Other Atoms) and Equivalent Isotropic Thermal Parameters (Å^2) (×10^2 for Metal Atoms, ×10 for Other Atoms) for Non-Hydrogen Atoms of $[(RhCp^*)_4V_6O_{19}]{\cdot}3CH_3CN{\cdot}H_2O$

atom	x	y	z	B_{eq}[a]
Rh(1)	19564 (11)	0	18191 (15)	245 (4)
Rh(2)	0	15971 (9)	54667 (15)	238 (4)
V(1)	10471 (16)	8557 (13)	36459 (22)	259 (6)
V(2)	0	0	55648 (46)	250 (13)
V(3)	0	0	17214 (45)	254 (13)
O(1)	0	0	3623 (16)	22 (5)
O(2)	881 (5)	710 (5)	2042 (7)	24 (2)
O(3)	866 (5)	719 (4)	5248 (7)	24 (2)
O(4)	1762 (8)	0	3602 (11)	24 (3)
O(5)	0	1422 (7)	3668 (11)	22 (3)
O(6)	1794 (6)	1465 (5)	3632 (9)	35 (3)
O(7)	0	0	352 (19)	39 (7)
O(8)	0	0	6966 (18)	36 (6)
C(1)	0	1965 (12)	7211 (21)	42 (7)
C(2)	768 (10)	2226 (7)	6626 (13)	38 (5)
C(3)	489 (10)	2669 (7)	5657 (13)	40 (5)
C(6)	0	1507 (15)	8269 (23)	80 (12)
C(7)	1725 (11)	2072 (10)	6945 (17)	59 (6)
C(8)	1073 (15)	3048 (9)	4816 (16)	62 (7)
C(11)	2437 (16)	0	82 (22)	46 (8)
C(12)	3279 (8)	406 (8)	1663 (13)	39 (5)
C(13)	2751 (10)	639 (9)	709 (14)	42 (5)
C(16)	1846 (20)	0	−995 (23)	71 (11)
C(17)	3732 (10)	877 (10)	2474 (16)	53 (6)
C(18)	2553 (13)	1412 (9)	393 (16)	58 (6)
N(1)	4373 (57)	0	5285 (49)	165 (51)
C(21)	2955 (27)	0	5910 (46)	50 (16)
C(22)	3435 (75)	0	5670 (64)	159 (45)
N(2)	0	−3157 (17)	−123 (29)	118 (14)
C(23)	0	−2312 (20)	1644 (28)	118 (18)
C(24)	0	−2767 (22)	696 (35)	112 (17)
O(w)	0	−5000	864 (46)	200 (28)

[a] $B_{eq} = (8\pi^2/3)\sum_{ij}U_{ij}a_i^*a_j^*\mathbf{a}_i{\cdot}\mathbf{a}_j$.

The structure was solved by direct methods (MULTAN78) and refined by block-diagonal least-squares technique with anisotropic thermal parameters for all non-hydrogen atoms. Atomic scattering factors and anomalous scattering corrections were taken from the reference.[31] The weighting scheme $w = [\sigma^2 + (0.04|F_o|)^2]^{-1}$ was employed. The final R and R_w values were 0.046 and 0.064 for 1484 independent reflections.

$[(RhCp^*)_3(IrCp^*)V_6O_{19}]{\cdot}3CH_3CN{\cdot}H_2O$ ($3{\cdot}3CH_3CN{\cdot}H_2O$). A black cubic crystal of cluster $3{\cdot}3CH_3CN{\cdot}H_2O$ (0.44 × 0.36 × 0.16 mm) recrystallized from acetonitrile was sealed in a manner similar to that above. Intensity data were collected on an Enraf-Nonius CAD4 diffractometer at 25 °C using graphite-monochromated Mo Kα radiation (λ = 0.71073 Å). Final lattice parameters were determined by least-squares treatment using the setting angles of 25 reflections in the range $25° < 2\theta < 30°$. Table I summarizes the crystal data and structure refinement results, and the other details are contained in the supplementary material. A total of 7878 reflections with $2\theta < 60°$ were collected with a θ–2θ scan. An empirical absorption correction with a set of ψ scans was applied. After corrections for absorption, decay (linear), and Lorentz and polarization effects, 5420 independent reflections were obtained on averaging in *Pmmn*, with the final data set consisting of 3432 unique observed reflections ($|F_o| > 6\sigma(F_o)$). Fractional coordinates are listed in Table III.

The structure was isomorphous with cluster **1**. The positions of the rhodium and iridium atoms occupying tetrahedral sites could not be distinguished due to their disorder. Accordingly, these atoms were refined with a scattering factor by $^3/_4$Rh + $^1/_4$Ir. The rhodium/iridium ratio was confirmed by the intensity ratio of the ^1H NMR signals of the C_5Me_5 groups and the ^{51}V NMR signals.

All calculations were carried out on a HITAC M680H computer at the Computer Center of the Institute for Molecular Science with the Universal Crystallographic Computation Program System UNICS-III.[32]

(25) This cation was generated similarly to $[(IrCp^*)(H_2O)_3]^{2+}$.
(26) ^1H NMR chemical shifts were referred to TMS in a capillary (the neat reference liquid added to a capillary inserted into an NMR tube containing the lock solvent) at 20 °C: (a) $[(RhCp^*)(D_2O)_3]^{2+}$ in D_2O, δ 1.03 (1.0×10^{-2} mol/dm^3); (b) cluster **1** in D_2O, δ 1.23 (1.0×10^{-2} mol/dm^3). The chemical shifts vary with sample concentration.
(27) (a) Hore, P. J. *J. Magn. Reson.* **1983**, *55*, 283. (b) Clore, G. M.; Kimber, B. J.; Gronenborn, A. M. *J. Magn. Reson.* **1983**, *54*, 170.
(28) Richens, D. T.; Helm, L.; Pittet, P.-A.; Merbach, A. E. *Inorg. Chim. Acta* **1987**, *132*, 85.
(29) Comba, P.; Helm, L. *Helv. Chim. Acta* **1988**, *71*, 1406.
(30) Day, V. W.; Klemperer, W. G.; Maltbie, D. J. *J. Am. Chem. Soc.* **1987**, *109*, 2991.
(31) *International Tables for X-ray Crystallography*; Kynoch Press: Birmingham, England, 1974; Vol. 4.
(32) Sakurai, T.; Kobayashi, K. *Rikagaku Kenkyusho Hokoku* **1979**, *55*, 69.

Table III. Fractional Coordinates ($\times 10^5$ for Metal Atoms, $\times 10^4$ for Other Atoms) and Equivalent Isotropic Thermal Parameters ($Å^2$) ($\times 10^2$ for Metal Atoms, $\times 10$ for Other Atoms) for Non-Hydrogen Atoms of $[(RhCp^*)_3(IrCp^*)V_6O_{19}]\cdot 3CH_3CN\cdot H_2O$

atom	x	y	z	B_{eq}[a]
M(1)	19571 (3)	0	18171 (5)	232 (1)
M(2)	0	15965 (3)	54702 (5)	254 (1)
V(1)	10464 (7)	8534 (6)	36463 (10)	246 (2)
V(2)	0	0	55662 (20)	249 (5)
V(3)	0	0	17236 (20)	251 (5)
O(1)	0	0	3641 (7)	19 (2)
O(2)	878 (3)	703 (2)	2050 (4)	24 (1)
O(3)	862 (3)	723 (2)	5252 (4)	24 (1)
O(4)	1750 (4)	0	3595 (5)	24 (1)
O(5)	0	1421 (3)	3663 (6)	25 (1)
O(6)	1791 (3)	1469 (3)	3641 (5)	36 (1)
O(7)	0	0	356 (9)	38 (3)
O(8)	0	0	6942 (9)	36 (3)
C(1)	0	1962 (5)	7196 (10)	38 (3)
C(2)	763 (6)	2233 (4)	6616 (7)	38 (2)
C(3)	472 (6)	2666 (4)	5688 (7)	42 (2)
C(6)	0	1494 (9)	8236 (13)	79 (6)
C(7)	1698 (7)	2061 (6)	6955 (11)	64 (3)
C(8)	1075 (9)	3048 (5)	4816 (10)	69 (4)
C(11)	2416 (8)	0	84 (10)	45 (3)
C(12)	3273 (4)	389 (4)	1613 (6)	37 (2)
C(13)	2754 (5)	634 (5)	679 (7)	40 (2)
C(16)	1827 (11)	0	−1023 (11)	73 (6)
C(17)	3718 (6)	880 (6)	2471 (9)	54 (3)
C(18)	2547 (7)	1389 (6)	401 (9)	61 (3)
N(1)	4531 (28)	0	5207 (28)	133 (20)
C(21)	2947 (13)	0	5872 (18)	38 (6)
C(22)	3647 (43)	0	5565 (32)	130 (21)
N(2)	0	3180 (11)	−226 (20)	142 (10)
C(23)	0	2345 (11)	1505 (16)	118 (10)
C(24)	0	2802 (10)	665 (18)	86 (7)
O(w)	0	5000	755 (29)	195 (17)

[a] $B_{eq} = (8\pi^2/3)\sum_{ij}U_{ij}a_i^*a_j^*\mathbf{a}_i\cdot\mathbf{a}_j$.

Results and Discussion

Synthesis. To assemble a model cluster for vanadium oxide surfaces interacting with MCp* (M = Rh, Ir) fragments, we used metavanadate VO_3^- as a building block of vanadium oxide parts and pentamethylcyclopentadienyl rhodium or iridium dichloride dimer $[MCp^*Cl_2]_2$ (M = Rh, Ir)[20] as a source of organometallic fragments. The MCp* group can accept three more ligand atoms, which define one face of an octahedron.[17] Treatment of $[MCp^*Cl_2]_2$ with $NaVO_3$ in water produces $[(MCp^*)_4V_6O_{19}]\cdot nH_2O$ (n = 4 for M = Rh (**1**·$4H_2O$) and 0 for Ir (**2**)) according to eq 1 in good yields (90–96%). Samples of **1** and **2** enriched

$$2[MCp^*Cl_2]_2 + 6NaVO_3 \xrightarrow{H_2O} [(MCp^*)_4V_6O_{19}]\cdot nH_2O + 6NaCl + 2HCl \quad (1)$$

with ^{17}O were prepared in ^{17}O-enriched water, with which VO_3^- readily exchanged oxygen under the experimental conditions. The use of orthovanadate VO_4^{3-} instead of VO_3^- leads to formation of[23,33] $[(MCp^*)_2(\mu\text{-}OH)_3]^+$ but not the clusters. The water of crystallization in **1**·$4H_2O$ is easily lost under vacuum at room temperature. Clusters **1** and **2** are air-stable both in solid and in solutions. In water, treatment of **1** with $[IrCp^*(H_2O)_3]^{2+}$ in a 1:1.3 molar ratio gives mainly $[(RhCp^*)_3(IrCp^*)V_6O_{19}]$ (**3**), as well as other minor products, $[(RhCp^*)_{4-n}(IrCp^*)_nV_6O_{19}]$ (n = 2, 3, 4) (see the paragraph on cluster **1** in solution).

Clusters in the Solid State. **1**·$3CH_3CN\cdot H_2O$ and **3**·$3CH_3CN\cdot H_2O$ are isostructural with each other. The structure of **1**·$3CH_3CN\cdot H_2O$ is shown in Figure 1. Table IV contains selected geometric information of both clusters. The clusters have a quadruple-cubane framework that contains four (MV_3O_4) cubic units alternatively fitted through V–O bonds at the three edges of the cube, and the central oxygen atom of the V_6O_{19} group is common to all four MV_3O_4 units; thus all oxygens of the V_6O_{19} group except for the terminal oxygens participate in the quadruple-cubane cluster (Figure 1). In another view, the clusters consist of one hexametalate $(V_6O_{19})^{8-}$ unit and four $(MCp^*)^{2+}$ groups situated on alternate faces of the octahedron that is formed by the hexavanadate unit through oxygen bridges (Figure 2). This structure has two crystallographic mirror planes perpendicular to each other: one contains Rh_{2i}, V_2, Rh_{2ii}, and V_3, while the other has the V_2, Rh_{1i}, V_3, and Rh_{1ii} atoms. These two planes cross at the central axis containing O_8, V_2, O_1, V_3, and O_7. The RhCp* and IrCp* groups in 3·$3CH_3CN\cdot H_2O$ are disordered with respect

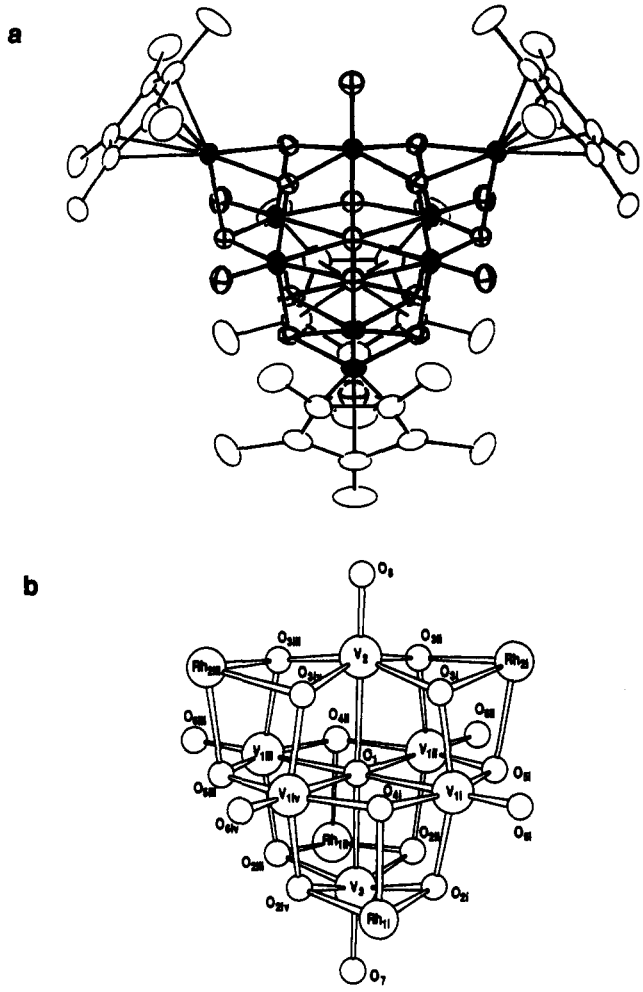

Figure 1. (a) ORTEP drawing of $[(RhCp^*)_4V_6O_{19}]$. The black-filled spheres represent metal atoms, bold-faced spheres represent oxygen atoms, and open ellipsoids represent carbon atoms. (b) Numbering scheme of $[(RhCp^*)_4V_6O_{19}]$. Carbon atoms are omitted for clarity.

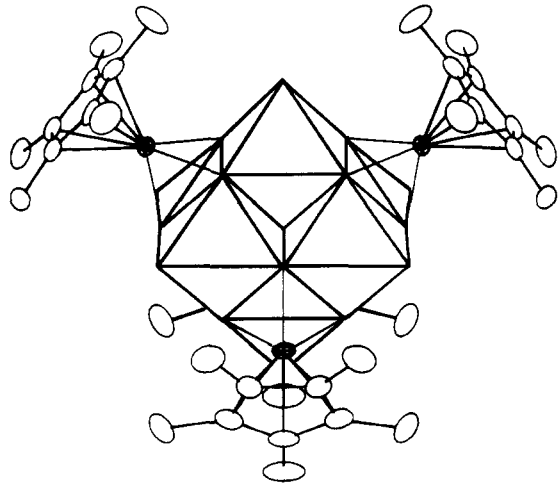

Figure 2. Polyhedra model for $[(RhCp^*)_4V_6O_{19}]$.

(33) Kang, J. W.; Maitlis, P. M. *J. Organomet. Chem.* **1971**, *30*, 127.

Table IV. Selected Bond Lengths and Angles for $[(RhCp^*)_{4-n}(IrCp^*)_nV_6O_{19}]\cdot 3CH_3CN\cdot H_2O$ (n = 0, 1)[a]

	n = 0	n = 1		n = 0	n = 1
Bond Lenghts (Å)					
M(1)–O(2i)	2.114 (8)	2.114 (4)	M(1)–C(11i)	2.16 (3)	2.14 (1)
M(1)–O(4i)	2.10 (1)	2.100 (6)	M(1)–C(12i)	2.15 (1)	2.136 (7)
M(2)–O(3i)	2.111 (8)	2.103 (4)	M(1)–C(13i)	2.13 (2)	2.150 (8)
M(2)–O(5i)	2.13 (1)	2.137 (7)	C(11i)–C(12i)	1.48 (2)	1.46 (1)
V(1i)–O(6i)	1.60 (1)	1.609 (5)	C(12i)–C(13i)	1.44 (2)	1.42 (1)
V(2)–O(8)	1.64 (2)	1.61 (1)	C(13i)–C(13iv)	1.51 (2)	1.45 (1)
V(3)–O(7)	1.60 (2)	1.60 (1)	C(11i)–C(16i)	1.54 (4)	1.57 (2)
V(1i)–O(1i)	2.248 (2)	2.246 (1)	C(12i)–C(17i)	1.46 (2)	1.52 (1)
V(1i)–O(2i)	1.910 (9)	1.903 (4)	C(13i)–C(18i)	1.52 (2)	1.48 (1)
V(1i)–O(3i)	1.908 (9)	1.912 (5)	M(2)–C(1i)	2.15 (2)	2.13 (1)
V(1i)–O(4i)	1.927 (7)	1.916 (4)	M(2)–C(2i)	2.14 (2)	2.130 (8)
V(1i)–O(5i)	1.905 (7)	1.907 (4)	M(2)–C(3i)	2.14 (1)	2.133 (7)
V(2i)–O(1i)	2.27 (2)	2.248 (9)	C(1i)–C(2i)	1.43 (2)	1.43 (1)
V(2i)–O(3)	1.910 (8)	1.913 (4)	C(2i)–C(3i)	1.46 (2)	1.42 (1)
V(3i)–O(1i)	2.22 (2)	2.240 (9)	C(3i)–C(3ii)	1.48 (2)	1.43 (1)
V(3i)–O(2i)	1.915 (8)	1.906 (4)	C(1i)–C(6i)	1.50 (4)	1.49 (2)
M(1)–M(1)	5.928 (2)	5.937 (1)	C(2i)–C(7i)	1.52 (2)	1.51 (1)
M(1)–M(2)	5.982 (2)	5.989 (1)	C(3i)–C(8i)	1.50 (2)	1.54 (1)
M(2)–M(2)	5.945 (2)	5.949 (2)	M(1)–V(1)	2.998 (3)	3.000 (1)
M(1)–V(3)	2.966 (2)	2.971 (1)	V(1i)–V(1ii)	3.173 (3)	3.175 (2)
V(1)–V(1iv)	3.185 (3)	3.180 (2)	V(1)–V(2)	3.175 (5)	3.174 (2)
V(1)–V(3)	3.179 (5)	3.177 (2)			
Bond Angles (deg)					
	n = 0	n = 1		n = 0	n = 1
O(2)–M(1)–O(4)	76.7 (3)	75.9 (2)	O(4)–V(1)–O(5)	157.8 (5)	157.5 (2)
O(2)–M(1)–O(2iv)	77.4 (3)	76.6 (2)	O(4)–V(1)–O(6)	100.9 (5)	101.6 (2)
O(3)–M(2)–O(5)	76.2 (3)	76.2 (2)	O(5)–V(1)–O(6)	101.3 (5)	100.9 (2)
O(3)–M(2)–O(3)	76.8 (3)	76.9 (2)	O(1)–V(2)–O(3)	78.8 (3)	79.0 (2)
O(1)–V(1)–O(2)	78.2 (6)	78.4 (3)	O(3)–V(2)–O(8)	101.2 (3)	101.1 (2)
O(1)–V(1)–O(3)	79.4 (6)	79.0 (3)	O(3i)–V(2)–O(3ii)	86.7 (4)	86.2 (2)
O(1)–V(1)–O(4)	79.1 (3)	78.8 (2)	O(3i)–V(2)–O(3iv)	89.0 (4)	89.6 (2)
O(1)–V(1)–O(5)	78.7 (3)	78.7 (2)	O(1)–V(3)–O(2)	78.7 (3)	78.5 (2)
O(1)–V(1)–O(6)	178.7 (6)	179.4 (3)	O(2)–V(3)–O(7)	101.3 (3)	101.5 (2)
O(2)–V(1)–O(3)	157.5 (4)	157.4 (2)	O(2i)–V(3)–O(2ii)	88.3 (4)	88.6 (2)
O(2)–V(1)–O(4)	86.0 (5)	85.5 (2)	O(2i)–V(3)–O(2iv)	87.3 (4)	86.8 (2)
O(2)–V(1)–O(5)	89.0 (5)	88.8 (2)			
O(2)–V(1)–O(6)	100.6 (5)	101.3 (2)			
O(3)–V(1)–O(4)	89.8 (5)	90.4 (2)			
O(3)–V(1)–O(5)	86.6 (5)	86.5 (2)			
O(3)–V(1)–O(6)	101.9 (5)	101.4 (2)			

[a] The Roman numerals stand for the numbering scheme of the symmetry operation.

to each other on the four alternate faces of the V_6O_{19} core. The four metal atoms in the MCp* units form a tetrahedral array (M_{1i}–M_{1ii} = 5.928 (2) Å in **1**·3$CH_3CN\cdot H_2O$ and 5.937 (1) Å in **3**·3$CH_3CN\cdot H_2O$), whereas the vanadium atoms are disposed in an octahedral arrangement (V_{1i}–V_{1ii} = 3.173 (3) Å in **1**·3$CH_3CN\cdot H_2O$ and 3.175 (2) Å in **3**·3$CH_3CN\cdot H_2O$) with bridging oxygens. The rhodium or iridium metal in the MCp* group is bound to three adjacent bridging O atoms (average M–O = 2.11 Å in **1**·3$CH_3CN\cdot H_2O$ and 2.11 Å in **3**·3$CH_3CN\cdot H_2O$) and assumes an octahedral geometry to achieve the 18-electron configuration, as observed previously.[8a,17] The vanadium atoms can be described as octahedrally coordinated through three distinct types of V–O bonds, one V–O^T, four V–O^B, and one V–O^C bonds (O^T, O^B, and O^C are terminal, bridging, and central oxygen atoms, respectively) and are displaced from the center of the octahedron toward the terminal oxygen. The bridging oxygens are closer to the central oxygen.[34] The geometry around the vanadium is quite similar to that in[35] $V_{10}O_{28}^{6-}$ and in vanadium oxide, V_2O_5.[36] The larger numbers of metal atoms bonding to the bridging oxygen implies longer V–O^B bonds. For example, the V–μ_3-O^B distances range from 1.905 to 1.927 Å and the V–μ_6-O^C distances from 2.22 to 2.27 Å in **1**·3$CH_3CN\cdot H_2O$. The O^B–M–O^B angles through the face of the cube depend on the kinds of chelated metals and the strength of the M–O bonds; the O^B–Rh–O^B angles range from 76.2° to 77.4°; the O^B–V–O^B angles, from 86.0° to 87.3°.

The hexametalate structure (M_6O_{19}) is one of the best known structures in polyoxometalates such as $Nb_6O_{19}^{8-}$, $Ta_6O_{19}^{8-}$, $Mo_6O_{19}^{2-}$, and $W_6O_{19}^{2-}$. The hexamer $V_6O_{19}^{8-}$, however, has not yet been prepared.[37] Thus **1** and **3** are the first examples including the vanadate hexamer. The V–O bond distances in **1**·3$CH_3CN\cdot H_2O$, and **3**·3$CH_3CN\cdot H_2O$ are compared with the M–O bond distances of $M_6O_{19}^{n-}$ (n = 8 or 2) in Table V, and the bond strength values of the M–O bonds and the valence sums at each metal atom in M_6O_{19} cores, as well as $V_{10}O_{28}^{6-}$, are computed from M–O bond distances in Table V and are summarized in Table VI.[38] The M–O^T bond strengths can be placed in the

(34) In addition to the noncentrosymmetry of the cluster molecules, the O–V–O asymmetry due to three distinct types of V–O bond and changes in bond polarizability with V–O distances contribute to the enhancement of nonlinear optic properties of clusters **1** and **3**. Actually, cluster **1** exhibits a relative harmonic intensity for second harmonic generation (SHG) of 1.6 times that of the urea standard used at 1.9 μm (130 MW/cm³) of a YAG laser (Kurtz powder test). The details of nonlinear optic properties of these and related oxide clusters will be reported elsewhere.

(35) Durif, P. A.; Averbuch-Pouchot, M. T.; Guitel, J. C. *Acta Crystallogr., Sect. B: Struct. Sci.* **1980**, *B36*, 680.

(36) Bachmann, H. G.; Ahmed, F. R.; Barnes, W. H. *Z. Kristallogr.* **1961**, *115*, 110.

(37) (a) Reference 13; pp 20–21. (b) Pope, M. T. In *Comprehensive Coordination Chemistry*; Wilkinson, G., Gillard, R. D., McCleverty, J. A., Eds.; Pergamon Press: Oxford, England, New York, 1987; Vol. 3, Chapter 38, p 1023.

(38) A valence-bond formalism has been applied to polyanion structures, and the bond strength value can be calculated by the equation of $S = (R/R_1)^{-N}$, where R is the metal–oxygen bond length and R_1 and N are empirical parameters introduced by Shannon. See: Reference 13; pp 20–21. Brown, I. D.; Shannon, R. D. *Acta Crystallogr., Sect. A: Found Crystallogr.* **1973**, *A29*, 266.

Table V. Mean Bond Lengths (Å) in the Hexametalate Core[a]

	ref	$M-O^T$	$M-O^C$	$M-O^B$
$(n\text{-}Bu_4N)_2[Mo_6O_{19}]$	48	1.677 (1.667–1.680)	2.318 (2.302–2.329)	1.925 (1.904–1.943)
$(n\text{-}Bu_4N)_2[W_6O_{19}]$	39	1.693 (1.672–1.713)	2.325 (2.321–2.333)	1.924 (1.892–1.948)
$Na_7(H_3O)[Nb_6O_{19}]\cdot 14H_2O$	49[b]	1.766 (1.752–1.780)	2.378 (2.370–2.386)	2.006 (1.970–2.055)
$[Ta_6O_{19}]^{8-}$	13	1.80	2.38	1.99
$[(RhCp^*)_4V_6O_{19}]\cdot 3CH_3CN\cdot H_2O$	*d*	1.61 (1.60–1.64)	2.25 (2.25–2.27)	1.913 (1.905–1.927)
$[(RhCp^*)_3(IrCp^*)V_6O_{19}]\cdot 3CH_3CN\cdot H_2O$	*d*	1.61 (1.60–1.61)	2.247 (2.246–2.248)	1.910 (1.903–1.916)
$(n\text{-}Bu_4N)_2[(RhCp^*)(cis\text{-}Nb_2W_4O_{19})]$[c]	8a	1.59 (1.24–1.78) 1.69 (1.68–1.71)	2.27 (2.25–2.29) 2.42 (2.41–2.46)	2.05 (1.98–2.10) 1.91 (1.86–1.93) 1.95 (1.90–1.94) 1.92 (1.85–2.00)

[a] Numerals in parentheses give the ranges of bond lengths found in the clusters. [b] The authors have suggested that the proton that is present in this niobate probably exists in the hydrated form H_3O^+. [c] Each M–O bond can be grouped in two or four classes because of its unsymmetrical structure. [d] This work.

Table VI. Bond Strengths of M–O and Valence Sums at Each Metal Atom in the Hexametalates

	Mo[a]	W[a]	V(1)[b]	V(2)[c]	Nb[d]	Ta[a]
$M-O^T$	1.98	2.04	1.72	1.70	1.48	1.33
$M-O^B$	0.97	0.95	0.71	0.91 0.55	0.77	0.81
$M-O^C$	0.28	0.30	0.31	0.32	0.32	0.33
valence sum	6.14	6.14	4.87	4.94	4.88	4.90

[a] These values are taken from ref 13. [b] This work. V(1) represents $1\cdot 3CH_3CN\cdot H_2O$. $3\cdot 3CH_3CN\cdot H_2O$ gives the same values as does $1\cdot 3CH_3CN\cdot H_2O$. [c] V(2) represents $V_{10}O_{28}^{6-}$, and these values are calculated from the data of ref 30. [d] These values are calculated from the data of ref 49.

following order: Mo ≈ W > V > Nb > Ta. On the other hand, the $M-O^C$ bond strengths are almost the same in all five compounds. The V–μ_2-O^B and V–μ_3-O^B bond strengths in $V_{10}O_{28}^{6-}$ have values 0.91 and 0.55, respectively, and this indicates that the binding of μ_2-O^B with another vanadium atom to form the V–μ_3-O^B bond reduces the strength and increases the negative charge (basicity) on the bridging oxygen atom. The binding of rhodium or iridium metal to the bridging oxygen also leads to the same effects.

In the M_6O_{19} polyanions, a pattern of trans bond length alternation for coplanar eight-membered M_4O_4 rings has been observed and discussed.[39] Although the alternation in the novel monocapped anionic cluster, $[RhCp^*(cis\text{-}Nb_2W_4O_{19})]^{2-}$ is enhanced by binding of one capping group $[RhCp^*]^{2+}$ to the $Nb_2W_4O_{19}$ moiety,[8a] clusters **1** and **3** have regular V–O bond distances in the planar V_4O_4 rings, V(1i)–O(4i)–V(1iv)–O(5iii)–V(1iii)–O(4ii)–V(1ii)–O(5i) and V(2)–O(3i)–V(1i)–O(2i)–V(3)–O(2iii)–V(1iii)–O(3iii).

This is probably due to symmetrical binding of four organometallic groups (approximate T_d symmetry), and consequently, the molecule locates on the two mirror planes. Thus, the variation of $V-O^B$ distances in these vanadium hexamers is smaller than those of well-known hexametalate anions, and the framework of V_6O_{19} in **1** and **3** is quite regular (Table V).

The acetonitrile in cluster **1** is located on alternate faces of the vanadium hexamer where the RhCp* groups are not located. One of the three acetonitrile molecules is crystallographically disordered. The carbon of the methyl group in the acetonitrile is oriented toward the center of each alternate face. The water molecule is located on the two mirror planes.

The patterns of the IR spectra of clusters **1** and **3** in the $V-O^T$ stretching (850–1000 cm^{-1}) and the $V-O^C$ stretching (480–500 cm^{-1}) regions are similar to those for $Mo_6O_{19}^{2-}$ and $W_6O_{19}^{2-}$,[40] but the absorption frequencies are lower by 20–30 cm^{-1} than those for $Mo_6O_{19}^{2-}$ and higher by 40–60 cm^{-1} than those for $W_6O_{19}^{2-}$. On the other hand, the absorption bands in the $V-O^B$ stretching (550–750-cm^{-1}) region differ from those for the Mo and W hexamers (see the IR data in Experimental Section). Cluster **2** shows an IR spectral pattern similar to those of clusters **1** and **3**, and this indicates that cluster **2** has the same quadruple-cubane structure.

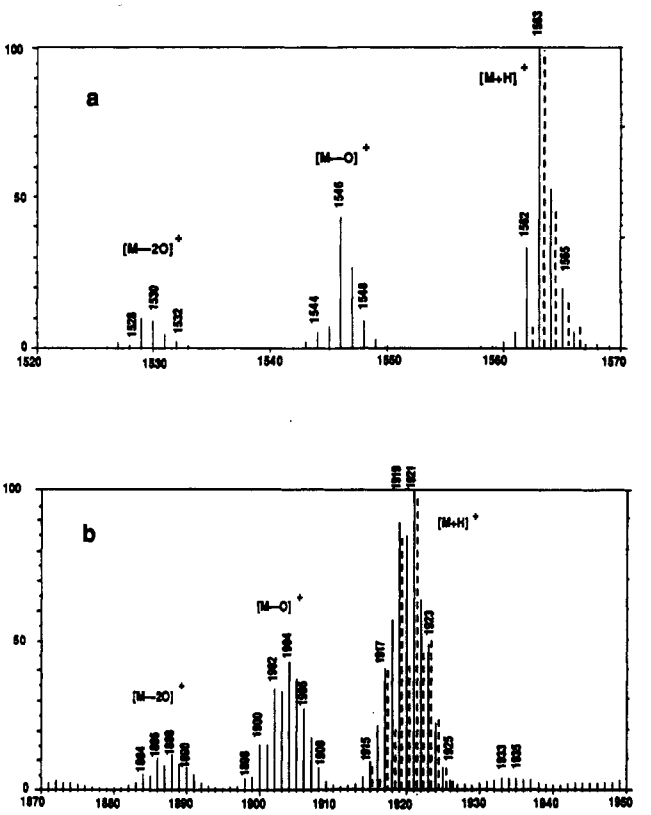

Figure 3. Positive-ion SIMS spectra of (a) $[(RhCp^*)_4V_6O_{19}]$ and (b) $[(IrCp^*)_4V_6O_{19}]$. The dotted lines are theoretical ion distributions of the molecular ion peaks.

The positive ion SIMS spectra of clusters **1** and **2** are shown in parts a and b of Figure 3, respectively. Both spectra contain the $[M + H]^+$ ions with characteristic isotopic distribution patterns and the most abundant mass ion peaks appear at m/z 1563 and 1921, respectively, as the base peaks. Interestingly, a major fragmentation pathway clearly displays sequential loss of oxygen atoms (m/z = 16) from these $[M + H]^+$ ions to form the $[M - O]^+$ and $[M - 2O]^+$ ions. A daughter ion search (B/E method) by a linked scan method revealed that the $[M + H]^+$ and [M –

(39) Fuchs, J.; Freiwald, W.; Hartl, H. *Acta Crystallogr., Sect. B: Struct. Sci.* **1978**, *B34*, 1764.
(40) Fuchs, J. *Z. Naturforsch.* **1973**, *28b*, 389.

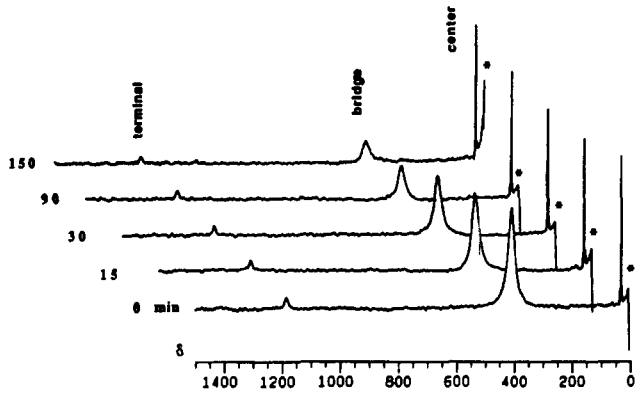

Figure 4. Arrayed ^{17}O NMR spectra of statistically ^{17}O-enriched cluster **1**, $[(RhCp^*)_4V_6O_{19}]$ in D_2O, illustrating the site-selective exchange reaction of oxygen with the time at 60 °C. An asterisk marks the surpressed signal of water.

$O]^+$ ions selectively produce the $[M - O]^+$ and $[M - 2O]^+$ ions, respectively. Thus, SIMS, as well as FABMS, is particularly noted for its outstanding sensitivity for chemical and isotopic detection, and it provides a rapid and accurate analytical method for determining the elemental composition and molecular weights of the oxide clusters.[41]

Cluster 1 in Solution. **1** is amphiphilic, soluble in dichloromethane, chloforom, toluene, and water,[42] but **2** is insoluble in water. Hence, cluster **1** is appropriate to study the comparative behavior of the cluster in both water and nonaqueous solvents. The ^1H NMR spectrum of cluster **1** shows a C_5Me_5 resonance at δ 1.939 (s) in $CDCl_3$ and δ 1.23 (s) in D_2O, and the ^{13}C NMR spectrum of **1** consists of two signals due to the C_5Me_5 ring at δ 93.72 (d, J_{Rh-C} = 8.9 Hz) and 9.44 (s) in $CDCl_3$ and δ 96.22 (d, J_{Rh-C} = 9.1 Hz) and 8.64 (s) in D_2O. The ^{17}O NMR spectrum of ^{17}O-enriched **1**-^{17}O displays three completely resolved signals at δ 1213 (half-width: 470 Hz), 386 (767 Hz), and 27 (12 Hz) in $CDCl_3$ and are assigned to the terminal, bridging, and central oxygens, respectively, on the basis of the general correlation between the chemical shift and the π-bond order of V–O.[43] The central oxygen has a narrow line width because its quadrupole relaxation time is longer than those of the other oxygen atoms, due to the higher symmetry of the former. The sample of **1**-^{17}O in D_2O at 20 °C also gives similar ^{17}O NMR signals at δ 1176 (half-width: 525 Hz), 404 (1192 Hz), and 27 (14 Hz), but the signal of the O^B is broader than the corresponding signal in $CDCl_3$. This broadening of the O^B signal is due to the interaction of the bridging oxygen atom with the free water molecule.

(a) Site-Selective Oxygen Exchange of Cluster 1 with Water. The ^{17}O NMR spectrum measured at 20 °C after standing at 90 °C for 4 h displayed an anomalous decrease in the O^B signal intensity, although the intensities of the O^T and O^C signals remained unaltered. Figure 4 shows the time-dependent ^{17}O NMR spectra of cluster **1** at 60 °C. The ^{51}V NMR spectra measured between 25 and 90 °C showed only one signal of which the chemical shift varies slightly with temperature (δ −511 with a 541-Hz half-width at 20 °C, δ −504 with a 183-Hz half-width at 90 °C). These results indicate that site-selective oxygen exchange with free water occurs at the bridging oxygen atoms without any skeletal change, as follows:

$$[(RhCp^*)_4V_6{}^{17}O^C(^{17}O^T)_6(^{17}O^B)_{12}] + H_2{}^{16}O \rightarrow [(RhCp^*)_4V_6{}^{17}O^C(^{17}O^T)_6(^{17}O^B)_{11}{}^{16}O^B] + H_2{}^{17}O \quad (2)$$

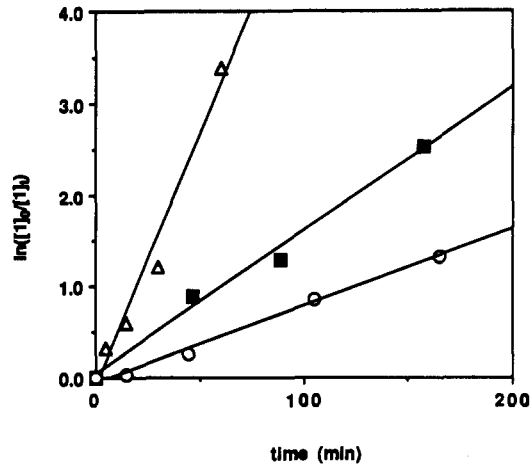

Figure 5. Plots of ln $([\mathbf{1}]_0/[\mathbf{1}]_t)$ vs time at (○) 60, (■) 70, and (△) 90 °C.

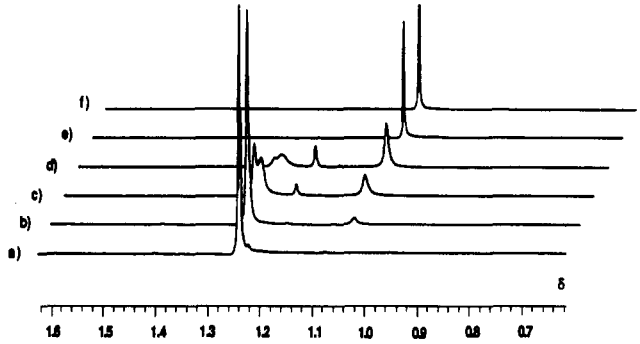

Figure 6. Arrayed ^1H NMR spectra of the methyl groups in $[(RhCp^*)_4V_6O_{19}]$ in D_2O, illustrating the dissociation reaction of $[RhCp^*]^{2+}$ groups as the pH of the solution decreases at 20 °C: (a) pH 7.1; (b) pH 4.8; (c) pH 3.8; (d) pH 2.8; (e) pH 1.6; (f) pH 1.0 (signals at δ 1.23 are due to cluster **1** and at δ 1.03 due to the dissociated $[RhCp^*(D_2O)_3]^{2+}$.

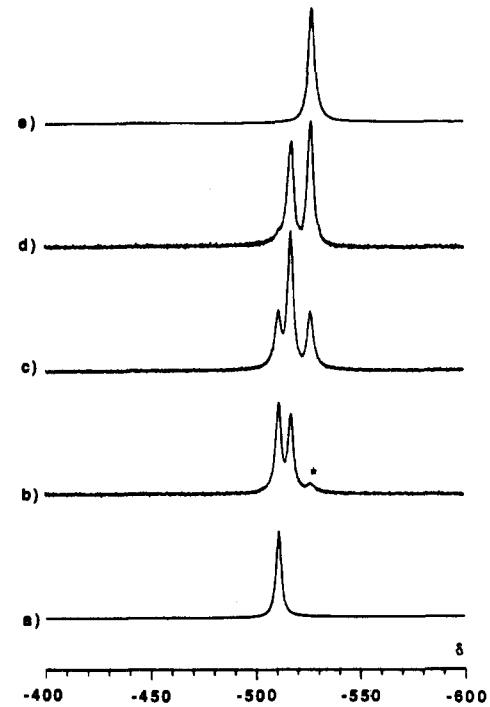

Figure 7. ^{51}V NMR spectra of clusters **1**–**5** in CD_2Cl_2 at 20 °C, showing the effect of substitution of organometallic groups. See Experimental Section for numerical data and experimental details. The asterisk marks the signal of an impurity.

The reverse reaction of eq 2 is ignored because the natural abundance of ^{17}O is very low (0.037%). This reaction is supposed

(41) (a) Finke, R. G.; Droege, M. W.; Cook, J. C.; Suslick, K. S. *J. Am. Chem. Soc.* **1984**, *106*, 5750. (b) Suslick, K. S.; Cook, J. C.; Rapko, B.; Droege, M. W.; Finke, R. G. *Inorg. Chem.* **1986**, *25*, 241 and references therein. (c) Lodding, A. In *Inorganic Mass Spectrometry*; Adams, F., Gijbels, R., Grieken, R. V., Eds.; John Wiley & Sons: New York, 1988; p 125.

(42) The molar conductivity of **1** is 36.9 S cm^2 mol^{-1} (1×10^{-3} mol/dm^3, 25 °C, pH 6.8).

(43) (a) Klemperer, W. G. *Angew. Chem., Int. Ed. Engl.* **1978**, *17*, 246. (b) Filowitz, M.; Ho, R. K. C.; Klemperer, W. G.; Shum, W. *Inorg. Chem.* **1979**, *18*, 93.

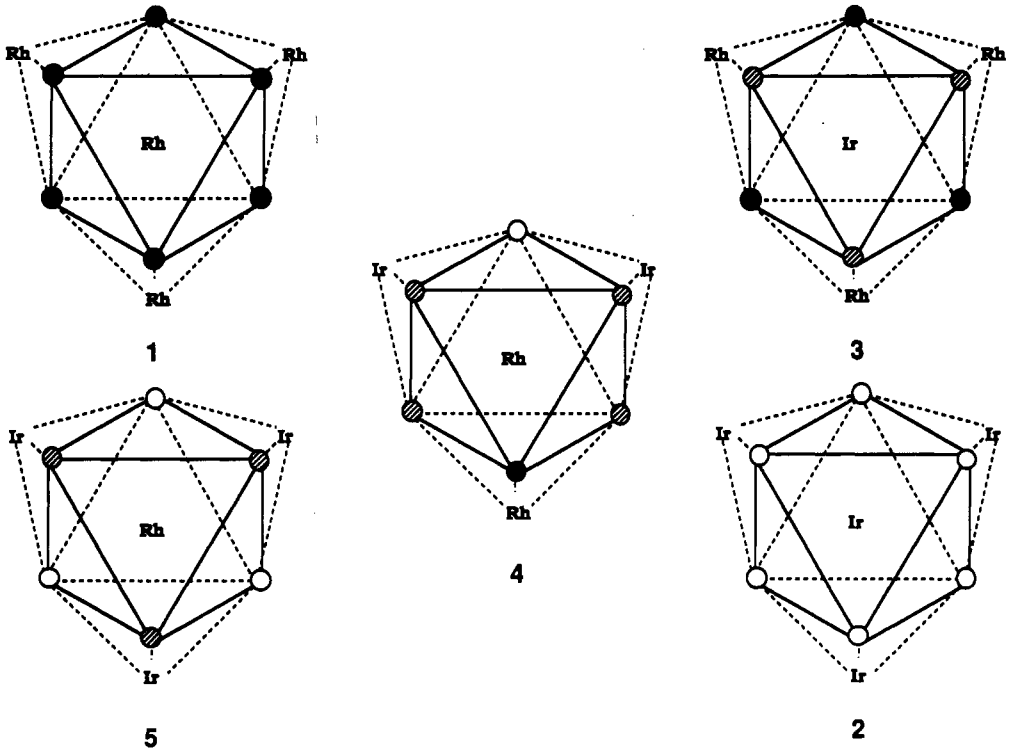

Figure 8. Skeletal representations of clusters **1**–**5**. Hydrogen, carbon, and oxygen atoms are omitted for clarity. Vanadium atoms are located at the corner of the polyhedron. The same chemical environments of the vanadium atoms are represented with identically marked circles.

to be irreversible, and pseudo-first-order conditions were assumed. The rate of the exchange was determined at 60, 70, and 90 °C by measuring the signal intensity of the O^B atoms in ^{17}O NMR spectra. Plots of ln $([\mathbf{1}]_0/[\mathbf{1}]_t)$ vs time were fit by standard linear regression techniques to obtain pseudo-first-order rate constants k_{obs} (1.4×10^{-4} s^{-1} at 60 °C, 2.6×10^{-4} s^{-1} at 70 °C, and 9.2×10^{-4} s^{-1} at 90 °C) (Figure 5). Approximate activation parameters for eq 2 are $\Delta H^{\ddagger} \cong 57$ kJ mol^{-1} and $\Delta S^{\ddagger} \cong -2$ J K^{-1}. The rate of exchange decreases with decreasing hydrogen ion concentration and increases dramatically below pH 4.5, where dissociation of the RhCp* group in **1** takes place; vide infra. Unfortunately, we were not able to change the concentration of the cluster in solution for the kinetic measurement because uncertainty in the intensity of the O^B NMR signal due to a high noise level was observed in more dilute solution.

Recent oxygen-exchange studies on the decavanadate have estimated that all structurally different types of oxygen atoms are kinetically similar. This oxygen-exchange experiment was explained on the basis of a "half-bonded intermediate" mechanism that involves cleavage of a V–O–V bridge in the decavanadate.[29,44] In $Mo_2O_4^{2+}$, the exchange rate of the terminal oxygen is faster than that of the bridging oxygen.[45] It was briefly reported that $Ta_6O_{19}^{8-}$ has three exchange rates corresponding to three oxygen sites with the following order, $O^T > O^B \gg O^C$.[43b] In our case, the bridging oxygen was selectively exchanged with water. These studies revealed that two main mechanisms that work in the oxygen exchange are a water-assisted dissociative path and a H^+-assisted path.[29,43] The important factors affecting the rate of the oxygen-exchange reaction are the bond strength of M–O, the basicity of oxygen, and the steric congestion around the M–O group. For $M_6O_{19}^{8-}$ it is expected to be ordered in M–O bond strength $M-O^T > M-O^B > M-O^C$, in basicity $O^C > O^B > O^T$, and in steric congestion $M-O^C \gg M-O^B \approx M-O^T$. The central oxygen in the framework of the cluster, which is stable in solution like cluster **1** and $Ta_6O_{19}^{8-}$, is hardly attacked by H^+ or H_2O because of steric congestion. Table VI indicates the $V-O^T$ in **1** is much stronger than the $Ta-O^T$ in $Ta_6O_{19}^{8-}$. The O^B atom in **1** is more basic than the corresponding oxygen in $Ta_6O_{19}^{8-}$. The capping organometallic groups in **1** inhibit formation of the cracking intermediate and prevent the solvent molecules from interacting with the terminal oxygen atoms. Therefore, the O^B in cluster **1** is much more susceptible to the exchange than the O^T, in contrast with that in $Ta_6O_{19}^{8-}$.

(b) Dissociation and Substitution of the RhCp* Groups in Cluster 1. The framework of cluster **1** is stable in both nonaqueous solvents and neutral water, but dissociation of the RhCp* group from **1** is observed in acidic aqueous solution and becomes appreciable around pH 3.8. Figure 6 shows the arrayed ^1H NMR spectra of cluster **1** taken at various pH values in D_2O at 20 °C. The methyl signal of the Cp* ring in cluster **1** appears at δ 1.23. As the acidity of the solution is increased, the signal intensity of cluster **1** is decreased and four kinds of new signals are observed at higher fields.[46] Under strong acidic conditions (pH 1–1.6), these signals are converged at δ 1.03. This resonance is due to the dissociated organometallic group $[(RhCp^*)(D_2O)_3]^{2+}$ that is confirmed from another experiment (see Experimental Section). From these results, the bridging oxygen atoms in cluster **1** must be protonated in an acidic aqueous solution, and this protonation causes the $(RhCp^*)^{2+}$ groups to dissociate (eq 3).

$$[(RhCp^*)_4V_6O_{19}] + 2n HBF_4 \rightleftarrows H_{2n}[(RhCp^*)_{4-n}V_6O_{19}] + n[(RhCp^*)(H_2O)_3](BF_4)_2 \quad (3)$$

Consequently, the charge density of the dissociated cluster $[(RhCp^*)_{4-n}V_6O_{19}]^{2n-}$ is increased, and the resonance of the Cp* groups was shifted toward a higher field. The distribution of the $[(RhCp^*)_{4-n}V_6O_{19}]^{2n-}$ species depends on the pH of solution. In the region of pH 3.8–2.8 all signals show line broadening caused by intermolecular exchange of $(RhCp^*)^{2+}$ groups between the dissociated species and free $[Cp^*Rh(D_2O)_3]^{2+}$, as observed previously for $[RhCp^*(Nb_2W_4O_{19})]^{2-}$.[8a]

By virtue of this dissociation, we can obtain mixed clusters of $[(RhCp^*)_{4-n}(IrCp^*)_nV_6O_{19}]$ (n = 1–3) from the reaction of **1** with $[IrCp^*(L)_3]^{2+}$ (L = H_2O or CH_3CN). The $(IrCp^*)^{2+}$ was added to an acidic solution of cluster **1** with HBF_4 to form a mixture of clusters $[(RhCp^*)_{4-n}(IrCp^*)_nV_6O_{19}]$ ($0 \le n \le 4$), which were

(44) Murmann, R. K.; Giese, K. C. *Inorg. Chem.* **1978**, *17*, 1160.
(45) Hinch, G. D.; Wycoff, D. E.; Murmann, R. K. *Polyhedron* **1986**, *5*, 487.
(46) The species with the methyl signal at δ 1.21 has been isolated as $[H_2(RhCp^*)_3V_6O_{19}]$, and its X-ray structure analysis is in progress now.

separated with a silica gel column. When the number of the IrCp* groups, n, is increased, the solubility of these clusters in water is decreased. The ^{1}H NMR spectrum of $[(RhCp^*)_{4-n}(IrCp^*)_nV_6O_{19}]$ ($0 \le n \le 4$) displays two resonances having relative intensities of $(4-n):n$ in the methyl region of the Cp* group, and the methyl signals of the IrCp* groups always appear at a higher field than that of the RhCp* groups. The chemical shift values of both methyl groups decrease with increasing number of n in $[(RhCp^*)_{4-n}(IrCp^*)_nV_6O_{19}]$. In the ^{13}C NMR spectra, two sets of the methyl and the ring carbon signals were observed at δ ca. 9.4 and 94.5 (d, J_{Rh-C} = 8.9 Hz) for RhCp*and δ ca. 9.9 and 87.0 for IrCp*, respectively. Figure 7 shows the ^{51}V NMR spectrum of clusters **1-5** in CD_2Cl_2. The ^{51}V NMR spectra of these substituted clusters show the difference in the chemical environment of the vanadium atoms clearly. When one IrCp* group is substituted for a RhCp* group, the resulting $[(RhCp^*)_3(IrCp^*)V_6O_{19}]$ has two equally intense signals. When two or three RhCp* groups are replaced, three or two signals are observed. These chemical environments around the vanadium atom of the substituted clusters are shown in Figure 8. The chemical environments are classified into three types: the first has two adjacent rhodium atoms (δ -511 to -512; filled circle in Figure 8), the second has one adjacent rhodium and iridium atoms (δ -517 to -518; dashed circle in Figure 8), and the third has two adjacent iridium atoms (δ -527 to -529; open circle in Figure 8). The intensity ratios of these signals are proportional to the number of vanadium atoms. The assignments were easily made by comparison of the NMR data of the substituted clusters, since the vanadium at the rhodium-coordinated site is more deshielded than that of the iridium-coordinated site. The line widths of the iridium-substituted clusters were found to be wider by 35-114 Hz than that of cluster **1**.

Conclusions. We have synthesized the organometallic oxide cluster $[(MCp^*)_4V_6O_{19}]$ (**1** and **2**) using VO_3^- and $[MCp^*Cl_2]_2$ as a model compound for the inorganic oxide-bound RhCp* groups, which is much more active and selective for hydroformylation.[15,16] The new quadruple-cubane framework, which contains a structure similar to the fragment structure of V_2O_5, has a more well-balanced structure in the solid state than the other hexametalates. This cluster has a fixed framework in organic solvents and a remarkable amphiphilic character in spite of being a neutral molecule with a quite large molecular weight. The discrete $V_6O_{19}^{8-}$ has not yet been prepared and is thought to be quite labile in solution,[29] but other $M_6O_{19}^{n-}$ types (n = 8, Nb, Ta; n = 2, Mo, W) have been isolated as some of the most stable polyoxoanions. This fact seems to be attributed to the smaller radii of V^{5+} (0.68 Å in coordination number (CN) 6), which interferes with the assembly of a cagelike structure with the VO_6 unit, compared with other metals in the same CN 6 (Nb^{5+}, 0.78 Å; Ta^{5+}, 0.78 Å; Mo^{6+}, 0.73 Å; W^{6+}, 0.74 Å).[47] The RhCp* groups balance the framework of the V_6O_{19} core by its symmetrical binding, and the Cp* groups sterically hinder attack of the solvent molecules in nonaqueous solvents. The exchange reaction of oxygen proceeds selectively at the bridging oxygen on heating in neutral aqueous solution, and the dissociation reaction of the organometallic groups takes place in acidic aqueous solution. The substitution reaction of the organometallic groups was performed by the introduction of other organometallic groups to an acidic solution of cluster **1**. That is a useful method to construct the cluster framework in a rational synthesis. In the case of the mixed cluster with the unavoidable disorder problems, the combination of X-ray crystallography and multinuclear NMR spectroscopy gives a good probe for revealing the structures of the mixed clusters.

Acknowledgment. This work was supported in part by Grant-in-Aid for Scientific Research No. 02804051 from the Ministry of Education, Science, and Culture of Japan. We also thank Mr. Kenichi Shizukuishi of Hitachi for measuring the SIMS spectra of the clusters.

Supplementary Material Available: A table of crystallographic data, an ORTEP diagram of cluster **3**, and tables of anisotropic temperature factors (4 pages); listings of observed and calculated structure factor amplitudes (30 pages). Ordering information is given on any current masthead page.

(47) Shannon, R. D. *Acta Crystallogr., Sect. A: Found Crystallogr.* **1976**, *A32*, 751.
(48) Dahlstrom, P.; Zubieta, J.; Neaves, B.; Dilworth, J. R. *Cryst. Struct. Commun.* **1982**, *11*, 463.
(49) Goiffon, A.; Philippot, E.; Maurin, M. *Rev. Chim. Miner.* **1980**, *17*, 466.

Contribution from the Laboratoire de Chimie des Métaux de Transition, Université Pierre et Marie Curie, 4 Place Jussieu, 75252 Paris Cedex 05, France

Control of Intramolecular Electron Transfer by a Chemical Reaction. The 4,4'-Azopyridine/1,2-Bis(4-pyridyl)hydrazine System

Jean-Pierre Launay,*,† Myriam Tourrel-Pagis, Jean-François Lipskier, Valérie Marvaud,† and Christian Joachim†

Received October 9, 1989

The complexation of 4,4'-azopyridine by the pentaammineruthenium(II) group is described. The metal sites are coordinated to the pyridyl nitrogen atoms and interact through the conjugated azo linkage. Upon oxidation, an intervalence absorption is detected, but it is unresolved with respect to the nearby metal-to-ligand charge-transfer band. The acidification of the binuclear pentaammineruthenium(II) complex gives rise to a pH induced intramolecular redox reaction yielding a ruthenium(III) complex of the reduced form of 4,4'-azopyridine, i.e. 1,2-bis(4-pyridyl)hydrazine. Reduction of the latter complex allows the investigation of intervalence transfer through 1,2-bis(4-pyridyl)hydrazine. It is found that the electronic interaction is greatly reduced in the reduced form of the ligand with respect to the oxidized form. This modification is discussed in the frame of an extended Huckel molecular orbital calculation.

Introduction

Intramolecular electron transfer is one of the basic processes involved in molecular electronics. Thus long molecules containing two redox sites linked by a conjugated pathway can be considered as "molecular wires".[1,2] To go further, it is necessary to devise molecules in which the electronic coupling could be modified by an external perturbation, thus playing the role of switches. A first possibility would be to change the geometry by a photophysical excitation, and such compounds are currently under investigation.[3]

† Present address: Centre d'Elaboration de Matériaux et d'Etudes Structurales, CNRS, 29 rue Jeanne Marvig, 31055 Toulouse Cedex, France.

(1) Arrhenius, T. S.; Blanchard-Desce, M.; Dvolaitzky, M.; Lehn, J. M.; Mathête, J. *Proc. Natl. Acad. Sci. U.S.A.* **1986**, *83*, 5355.
(2) Woitellier, S.; Launay, J. P.; Spangler, C. W. *Inorg. Chem.* **1989**, *28*, 758.

0020-1669/91/1330-1033$02.50/0